Honda Research Institute EU
Honda Research Institute Europe GmbH
https://www.honda-ri.de/

A Novel Transonic Fan Swept Outlet Guide Vane Using 3D Design Optimization

Giles Endicott, Markus Olhofer, Toshiyuki Arima, Toyotaka Sonoda

2014

Preprint:

This is an accepted article published in Proceedings of the ASME Turbo Expo (ASME). The final authenticated version is available online at: https://doi.org/[DOI not available]

Proceedings of ASME Turbo Expo 2014: Turbine Technical Conference and Exposition
GT2014
June 16 – 20, 2014, Düsseldorf, Germany

DRAFT GT2014-25857

A NOVEL TRANSONIC FAN SWEPT OUTLET GUIDE VANE USING 3D DESIGN OPTIMIZATION

Toyotaka Sonoda
Honda R&D Co., Ltd.
Aircraft Engine R&D Center
Wako-shi, Saitama 351-0193, Japan

Giles Endicott
Honda Research Institute Europe GmbH
Carl-Legien-Str.30
D-63073 Offenbach/Main, Germany

Toshiyuki Arima
Honda R&D Co., Ltd.
Automobile R&D Center
Wako-shi, Saitama 351-0193, Japan

Markus Olhofer
Honda Research Institute Europe GmbH
Carl-Legien-Str.30
D-63073 Offenbach/Main, Germany

ABSTRACT

In our previous work on a transonic fan swept outlet guide vane (OGV) for a small turbofan engine (GT2011-46363), we showed a novel oscillatory casing profile that leads to approximately 20% loss reduction, using a numerical design optimization method. In this paper we analyze the resulting geometry of an optimization based on a blade representation which is able to realize significantly larger surface modifications. The final optimized design displays a novel blade geometry that has its maximum blade thickness at around 80% blade chord (located between the blade's mid-chord and trailing edge) especially in the mid-span region. The flow physics explaining why this blade geometry without the oscillatory casing profile has the same loss reduction level of more than 20% at the peak efficiency point are discussed, focusing on the secondary flow and span-wise static pressure gradient on the blade suction side.

NOMENCLATURE

Cp	specific heat at constant pressure
M	Mach number
p	static pressure
Po	total pressure
R	gas constant
RT	circumferential distance
r	distance in radial direction
To	total temperature
Tu	free-stream turbulent intensity
U	blade speed
v	flow velocity
X	distance in axial direction
γ	ratio of specific heat capacities Cp/Cv
ρ	density
μ_T/μ	eddy viscosity ratio

Subscripts

1	inlet station upstream of the rotor leading edge
2	outlet station of rotor / inlet station of the OGV
3	outlet station downstream of the OGV
tip	blade tip
θ	angle in circumferential direction

Abbreviations

CFD	computational fluid dynamics
EXP	experiment
FFD	free form deformation
LE	leading edge
OGV	outlet guide vane
PS	pressure surface
SS	suction surface
TE	trailing edge

INTRODUCTION

Aviation gas turbines have reaped the benefits of adding a bypass system to their design through extracting energy from their exhaust stream to power a high mass flow fan. In doing so, these engines increase their propulsive efficiency, that is, the ratio of the propulsive power to the power contained in the exhaust jet and additionally they significantly reduce the amount of noise produced by the expelled exhaust jet. Due to the relationship between exhaust velocity and propulsive

Copyright © 2014 by ASME

efficiency, the ratio of air passing through the bypass fan system undergoing only a modest velocity increase compared to the core engine has increased in the past decades to increase efficiency further.

At the historic onset of the turbofan, the bypass ratio was roughly one, today it is closer to ten. The fan rotor, powered by a low pressure turbine within the core engine increases the stagnation pressure of the incoming air from the upstream diffuser. In doing work on the air, the rotor imparts a significant angular velocity component, in accordance with the Euler work equation, which does not contribute to thrust. The energy contained in the angular velocity component can be converted to useful thrust by deflecting it to the axial direction in the downstream OGVs. Significant considerations of the design of OGVs have been performed in past decades, studying blade shape, lean, sweep [1-3] together with the shape of the passage that contains them, in both symmetrical and asymmetrical forms [4].

The compressor stage under investigation in this study is located within the fan stage of a modern small turbofan engine for a very light business jet. We concentrate on the design improvement of the OGVs. Initially we perform experimental testing on a small scale rig to ascertain the current design performance. Using computational fluid dynamics, we present a simulation strategy capable of simulating the flow-field around the OGVs. We move on to critically compare and contrast the experimental and computational results, with the aim of being able to confidently use the computational simulations to accurately create a testing environment for a new OGV design concept.

The application of computational design optimization can lead to significant improvements to in service performance without the need for intensive human intervention. Computational design or design optimization, pioneered in the aerospace domain in 1978 [5] with the numerical design of transonic wings has progressed to a popular technique for the development of turbomachinery in the current era. While early simulation methodologies pushed computational resources to their limits, allowing only several simulations to be performed in a given time frame, today steady state simulations are easily within the reach of commodity hardware, allowing numerical optimization technologies to be applied to the results of simulations.

We have already demonstrated that such a technology is very effective to find new design concepts which deliver an increased aerodynamic performance. For example, regarding the two dimensional compressor airfoil, an extreme front loading compressor cascade is very effective for the total pressure loss reduction, especially for a low Reynolds number regime, as compared to conventional controlled diffusion airfoils (CDA) [6, 7]. A novel oscillatory casing profile is described in [8] for a three dimensional compressor OGV, which is effective to reduce losses for a swept OGV. Due to constraints in the chosen representation of free form deformation (FFD), the achievable modifications of the blade were small, with the result that no alternative design concept for the blade geometry could be identified.

Therefore, the main objective in the work we describe in this paper is to seek a new design concept related to the OGV blade geometry itself, by allowing a larger level of blade modifications utilizing a geometric surface representation.

EXPERIMENTAL METHODS

The first stage of the design process was to accurately gauge the existing performance to form a benchmark from which to improve. In our case, such a process is best performed experimentally to ensure accuracy. The experiments were performed in a small scale high-speed single stage research compressor at the Honda Aircraft Engine R&D Center (see Figure 1). At the peak stage efficiency point in the cruise speed line the OGV loss is minimum (there are several black solid circles in Figure 6) and the inlet Mach number and the turning angle at the hub are approximately 0.9 and about 50 degrees, while at the tip they are approximately 0.7 and about 55 degrees. In order to reduce the shock loss at the hub the OGV leading edge was swept forward toward the hub. At the tip the OGV leading edge was swept forward again in order to increase solidity. The solidities at the hub and the tip are 2.8 and 1.8, respectively.

In the experimental rig, ambient air is led through a bell-mouth and a settling chamber with flow conditioning screens and a contraction before entering the compressor stage. The rotor is driven by a 300KW DC-drive with the shaft speed and power measured using a torque-meter. The mass flow rate is measured at the bell-mouth while the inlet total pressure and temperature are measured by probes located inside the settling chamber. The stage exit total pressure and temperature are measured by tandem probes located downstream of the OGV. Two tandem probes for total pressure measurements and two tandem probes for total temperature measurements are circumferentially distributed and traversed in the circumferential direction by a traversing ring concurrently in order to estimate the circumferential variation of the experiments. The OGV exit flow angle is obtained from a single five-hole probe installed into the traverse ring, so the probe can be circumferentially traversed at each span-wise position. Simultaneous measurements using the tandem probes and the five-hole probe were not possible, therefore they were carried out separately. As the compressor characteristics are significantly changed when the probes are inserted in the passage downstream of the rotor and upstream of the OGV, only static pressure at the casing wall was measured between the rotor-TE and OGV-LE. As a result of having no flow-field measurements between the rotor and OGV, the inlet boundary conditions for the OGV blade need to be predicted using the measured data together with some assumptions. The inlet total pressure of the OGV was assumed to be equal to be the maximum value of the OGV wake. On the other hand, the inlet total temperature of the OGV was assumed to be equal to be the mass averaged value of the OGV wake. These assumptions have been also used by Wennerstrom's high through flow

 Copyright © 2014 by ASME

transonic axial compressor stage [9] where the similarly swept OGV has been installed and tested. Also, the OGV-CFD results show that this assumption on the "inlet total pressure" is reasonable (not shown here). It therefore seems that the sweep incorporated in the OGV leading edge around the hub appears to entirely eliminate shock losses. The inlet flow angle of the OGV was calculated by applying the Euler turbine equation to the rotor and the simple radial equilibrium equation to the OGV inlet using an iterative procedure. This is as follows:

(1) Set $To_2(r) = To_3(r),\ Po_2(r) = Po_3(r)$.

(2) Calculate $v_{2\theta}(r)$ profile using

$$Cp\left(To_2(r) - To_1(r)\right) = U_2 v_{2\theta}(r) - U_1 v_{1\theta}(r).$$

(3) Assume pressure profile $p_2(r)$.

(4) Compute Mach number profile $M_2(r)$ using

$$M_2(r) = \sqrt{\frac{2}{\gamma - 1}\left\{1 - \left(\frac{Po_2(r)}{P_2(r)}\right)^{\frac{\gamma-1}{\gamma}}\right\}}.$$

(5) Compute density profile $\rho_2(r)$ using

$$\rho_2(r) = \left(\frac{Po_2(r)}{R \cdot To_2(r)}\right) \Bigg/ \left(1 + \frac{\gamma - 1}{2} M_2^{\,2}(r)\right)^{\frac{1}{\gamma-1}}.$$

(6) Update pressure profile $p_2(r)$ using

$$p_2(r) = p(r_{tip}) - \int_r^{r_{tip}} \rho_2(r) \frac{v_{2\theta}^{\,2}(r)}{r} dr.$$

(7) If pressure profile is not converged then repeat from step (4)-(6).

The measurement accuracy is, as follows. The loss coefficient uncertainty for a single wake measurement is determined to be ± 0.1 percent. However, due to circumferential variability of the wake, the maximum uncertainty for the overall mass averaged loss coefficient from P1 (near choke, see Figure 7) to P5 (near surge, see Figure 7) is estimated as ± 0.6 percent. For the exit flow angle is ± 0.5 degree.

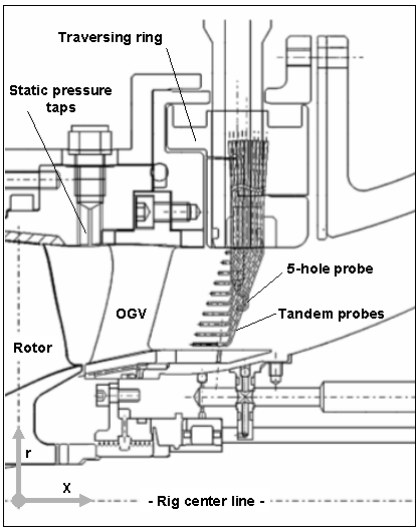

Figure 1: Small scale high-speed single stage research fan compressor rig.

COMPUTATIONAL METHODS

For the simulation of the fluid dynamic properties of the blade designs the parallelized 3D in-house Reynolds-averaged Navier-Stokes (RANS) flow solver HSTAR (Honda Software for Turbomachinery Aerodynamics Research) [10] was used. For turbulence modeling, Menter's k-ω SST turbulence model [11] was chosen because it gave the best agreement between CFD and experimental data for the baseline blade geometry.

As pointed out by Rumsey and Spalart [12], the k-ω SST model has a well-defined transition location for limited range of free-stream turbulent intensity (Tu), eddy viscosity ratio (μ_T/μ), and free-stream Mach number, however it is incapable of predicting re-laminarization. The boundary conditions for the turbulence model are modeled based on inlet turbulence levels, namely, Tu=5% and μ_T/μ=100. Such a high level of free stream turbulence leads to turbulent boundary layers immediately at the blade leading edge and on the casing walls.

In order to sufficiently resolve the boundary layer development, CFD simulations were performed in advance to determine the number of cells required to obtain grid independence. The chosen computational grid consisted of 201 nodes in the stream-wise direction, 81 nodes in the radial direction, and 61 nodes in the circumferential direction (totaling approximately one million cells). The average y^+ of the first grid point from the wall (both blade and end-wall) is close to 1.0 for all calculations.

The computational OGV grid for the baseline blade used in the simultaneous optimization of both airfoil and axisymmetric end-wall contouring outlined in [8] is shown in Figure 3. The grid for the tip end-wall part is intentionally shifted to the blade mid-span position in order to show a fine grid feature around the blade tip region. Flow direction is from "left" to "right" and the position of station 2 and 3 are the inlet and outlet stations of

Copyright © 2014 by ASME

the swept OGV, respectively. Also the detail grid at the airfoil frontal part is shown in Figure 3.

For the inlet boundary condition, the span-wise distribution of total pressure, total temperature and flow angle, obtained from the small scale rig testing, are set. The normalized overall span-wise total pressure distribution and the boundary layer thickness just upstream of the LE is shown in Fig. 4-left and right, together with the inlet total pressure boundary condition obtained from EXP,. In the right figure, the hub region (0% to 5% span-height) of the left figure is enlarged. It can be seen that the boundary layer thickness is about 1% of span-height.

For the outlet boundary condition, the same (constant) exit static pressure is applied to all cases (Baseline, OPT1 and OPT2).

The computation for one flow analysis with this grid takes roughly 50 minutes on an Intel Xeon5570 2.93 GHz Quad-Core processor using the Intel MPI library.

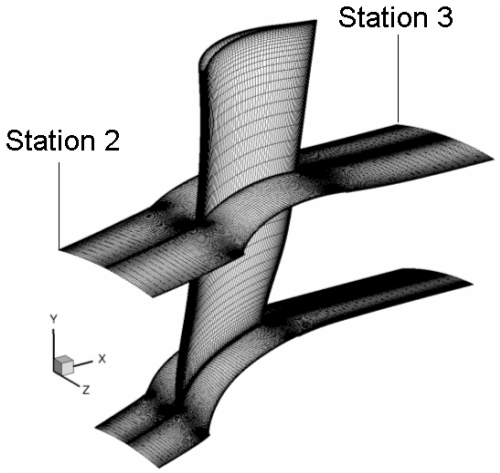

Figure 2: Structured computational grid for overall view.

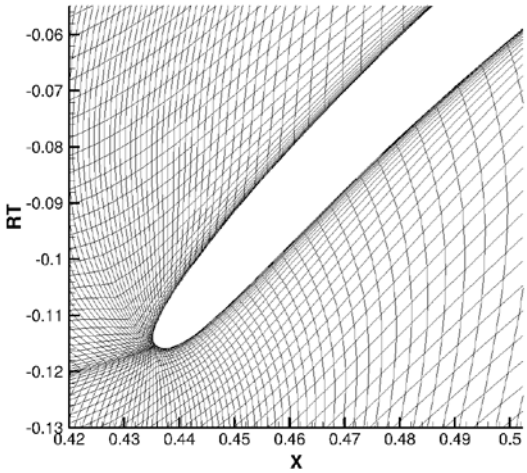

Figure 3: Structured computational grid for frontal part of baseline OGV at 5% span-height.

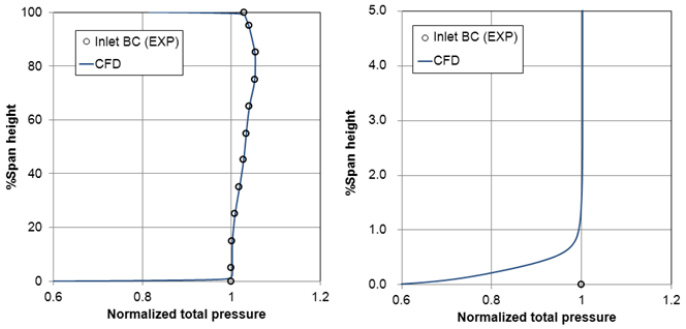

Figure 4: Inlet boundary layer thickness just upstream of OGV LE at P2, cruise speed-line, together with the inlet total pressure boundary condition based on EXP.

OPTIMIZATION METHODS

The OGV design optimization considered the pressure loss in the flow at three operation conditions in order to reflect different flight conditions of the engine. One design point reflects the conditions near peak efficiency, denoted as operation point P2, one reflects conditions at near choke, denoted as P1 and a last reflects conditions near surge and is denoted as P5 as also indicated in Figure 6, in which all data points are normalized by the loss value of the peak efficiency point measured in the experiment. Each value for the OGV losses has been obtained from the overall (both circumferential and span-wise) mass averaged total pressure loss coefficient.

Blade representation:

For the optimization, the blade shape is represented by 5 two dimensional profile cross sections. Each of the cross sections is defined by 13 parameters in total. Six parameters define 3 points along the camber mean-line which is represented by a spline. This spline is in addition to the three points fixed by the leading and trailing edge of the blade. Three parameters define the blade thickness at the position of the three points defining the main chamber spline. Furthermore there are parameters defining the leading edge radius, the stagger angle and the lean of the blade realized by a translation of the two dimensional cross section of the blade. One additional parameter in each cross section describes the distance of the leading edge thickness measurement point to the leading edge. During the optimization this parameter is adapted for the two blade cross sections closest to the hub and tip independent from each other, while the parameter in the remaining three cross section get the identical value represented by one single optimization parameter. In total three optimization parameters defined this blade parameter in all five cross sections. One additional parameter defined a corresponding value at the trailing edge.

In addition there are 3 parameters defining the casing at hub and 3 parameters defining the casing at the tip of the blade. In this way the blade and casing was defined by 70 design parameters which were subject to the optimization. The three

Copyright © 2014 by ASME

dimensional surface mesh of the blade as well as the surface mesh of the casing is generated by Catia V5 utilizing a parameterized blade and casing model defining the geometries by surface splines (see Figure **5**).

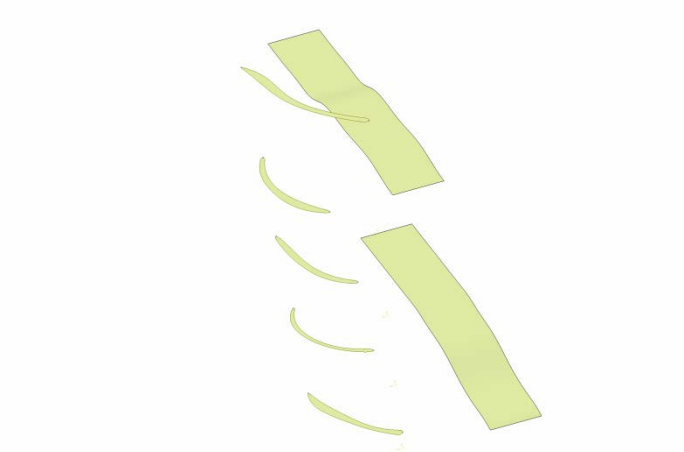

Figure 5: Sketch of the geometric model representing 5 blade cross sections as well as casing surfaces.

Constraints and objective function:

In the quality calculation three different types of constraints were applied. While the pressure loss $\omega_{P_2}^i$ of blade i at design point $P2$, representing the peak efficiency point defined the optimisation criteria, the pressure loss $\omega_{P_1}^i$ and $\omega_{P_5}^i$ at the other design points $P1$ and $P5$ define constraints in the sense that the performance at these points have to be at least as good as for the baseline. In case the pressure loss ω_{p1}^i was higher than the corresponding loss at the baseline blade $\omega_{p1}^{baseline}$ a penalty value p_{P_1} was added to the overall blade quality value where

$$p_{P_1} = \begin{cases} \omega_{p1}^i - \omega_{p1}^{baseline} & if\ \omega_{p1}^i - \omega_{p1}^{baseline} > 0 \\ 0 & otherwise \end{cases}.$$

For design point $P5$ a penalty value p_{P_5} was calculated in an identical manner.

In order to guarantee outflow angle α within given tolerances, a constraint was introduced evaluating the averaged angle along the blade. An average square value of outflow angle should be smaller than 2.0 which results in an averaged exit flow angle variation of about ±1.4 degree. The penalty term p_α was added to the solution quality value defined as

$$\bar{\alpha}^i = \frac{1}{N}\sum_{n=0}^{N}(\alpha_n^i)^2$$

$$p_\alpha^i = \begin{cases} \bar{\alpha}^i - 2 & if\ \bar{\alpha}^i > 2 \\ 0 & otherwise \end{cases}.$$

The overall quality Q^i of solution i is calculated by

$$Q^i = \omega_{P_2}^i + 10\, p_{P_1}^i + 10\, p_{P_5}^i + 5\, p_\alpha^i.$$

The weighting coefficients were determined empirically. Furthermore geometric constraints to the thickness of the blade cross sections were applied in order to guarantee a blade shape with the maximum thickness not smaller than the baseline geometry which was used for the experimental measurements as well and where realized by truncation of the thickness parameters in case smaller thickness values were generated by the optimization algorithm.

Optimization Algorithm:

All parameter were optimized by a particle swarm optimization [13] method. The population size of the swarm was chosen to be 50 with an acceleration of 1.7 and a decay of 0.6 which was determined empirically.

RESULTS AND DISCUSSION

Assessment of Flow Solver

The comparison between physical experimentation and simulations (CFD) of both the circumferential and span-wise averaged total pressure loss for the baseline OGV is shown in Figure 6. The black solid circles are the experimental values and the black open circles are the results of CFD. The vertical axis of the OGV total pressure loss and the horizontal axis of the mass flow rate are normalized by experimental value of the baseline overall OGV total pressure loss and the mass flow rate at the design point P_2 for cruise operating condition. It can be seen that there is a sudden increase of loss near the choke side, whereas a gradual increase of the loss can be observed near the stall side. In general, there is a very good qualitative and quantitative agreement between experimental and computational results. Further details on the assessment of the CFD solver, for example, span-wise OGV total pressure loss distributions at design and off-design points, are shown in [14].

Characteristics of Optimized OGV (OPT2)

In this section we discuss the results of the optimization process and report the aerodynamic characteristics of the best design found by the optimization process. In Figure 6 the present optimized OGV (called "OPT2") loss is shown as the red diamond shape, in comparison with the baseline. Also our previous optimized results (called OPT1, obtained from Ref. [8]) where the OGV geometry modification is smaller due to restrictions introduced by the applied deformation method is shown as the blue triangle shape. The present optimal design (OPT2), shows an improvement of about 30% in terms of total pressure loss reduction at the peak efficiency point P2 and is superior to OPT1 (20%). At the same time the loss level near stall condition is almost the same as that of the baseline due to the definition of the quality function.

Copyright © 2014 by ASME

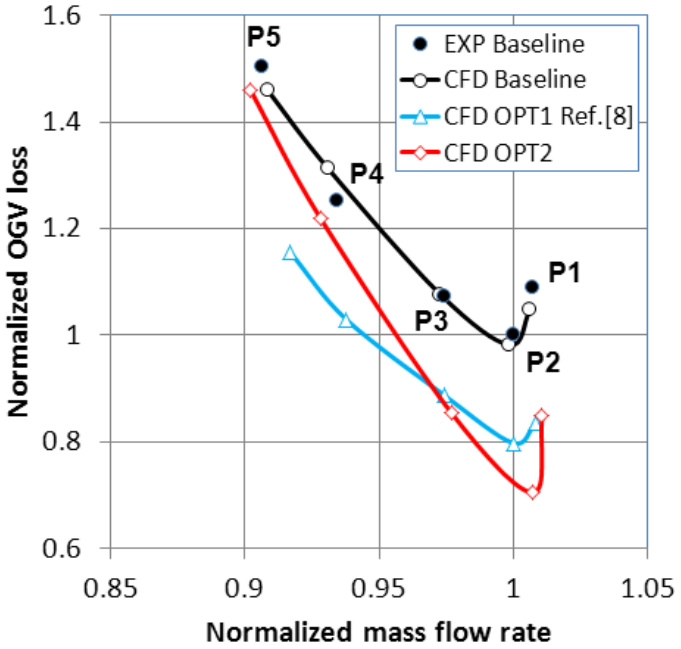

Figure 6: OGV loss characteristics at cruise speed-line for baseline (black line), OPT1 (blue line, Ref. [8]) and OPT2 (red line).

The three dimensional shape of the present optimal blade (OPT2) and the cross section blade geometry at mid-span are shown in Figure 7 and Figure 8, respectively. The most interesting point in Figure 8 is, that the frontal part of the airfoil is just like a curved plate and the maximum thickness is located at the rear part of the airfoil. The geometry is very novel and quite different from a controlled diffusion airfoil (CDA). The hub and tip section geometry is similar to the controlled diffusion airfoil (not shown here).

The passage geometry of the present optimization results (OPT2) is shown in Figure 9 (red line), in comparison with the baseline (black line) and OPT1 (blue line). In opposite to the design represented by OPT 1 no oscillatory casing profile appears in the optimization process. The OGV exit tip and hub radius for OPT2 are slightly different from the baseline, but this is not discussed in detail in this paper.

The span-wise loss distribution for the present optimization (OPT2) at the peak efficiency point (Point 2 in Figure 6) is shown in Figure 9, in comparison with the baseline and OPT1. Also there are experimental data for the baseline obtained from two different circumferential positions (wake1 & wake2). Comparing the baseline CFD results with the experimental data there is a relatively good qualitative agreement except for the hub region. In the case of the present optimization (OPT2) the loss is improved between 10% and 95% span-height in comparison to the baseline and between 10% and 60% span-height in comparison to OPT1.

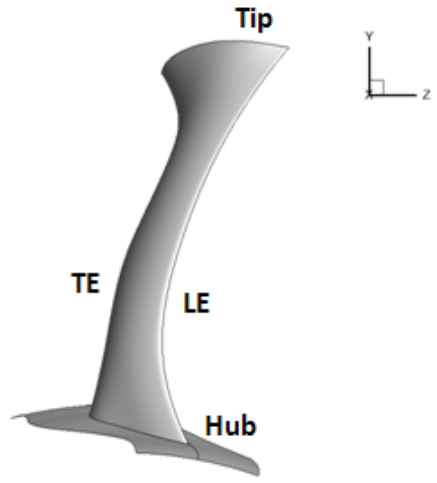

Figure 7: Overview of optimized OGV (OPT2).

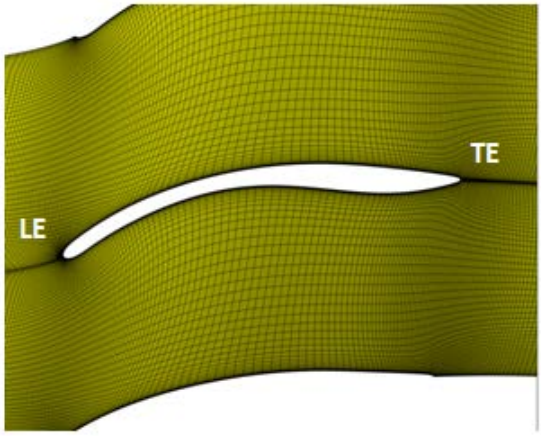

Figure 8: Cross section geometry at mid-span for present optimized OGV (OPT2).

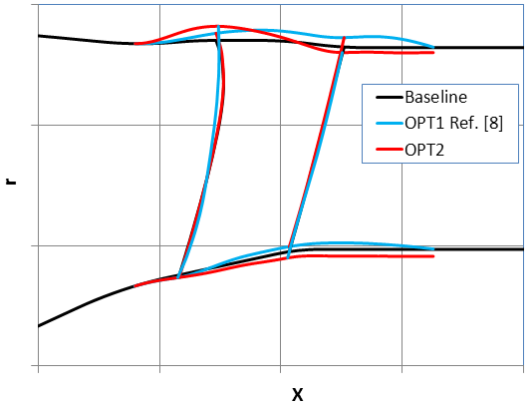

Figure 9: Comparison of passage geometry for baseline (black line), OPT1 (blue line, Ref. [8]) and OPT2 (red line).

Copyright © 2014 by ASME

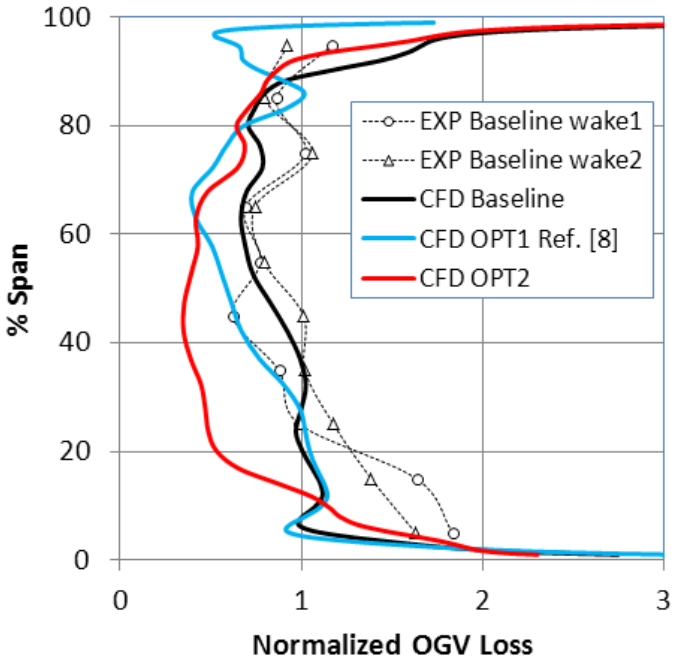

Figure 10: Comparison of span-wise loss distribution at P2, cruise speed-line, for baseline (black line), OPT1 (blue line, Ref. [8]) and OPT2 (red line).

The reason why OPT2 is superior at P2 (Point 2)

In this section, we discuss the reason why OPT2 has a low loss between about 10% and 60% span height observed in Figure 10, as compared to our previous optimized results (OPT1). The isentropic Mach number distribution on the airfoil surface at the peak efficiency condition (P2) for 10, 50, and 90% span height for both the baseline blade and the optimized blades (OPT1 & OPT2) is shown in Figure 11. The most interesting point is that the blade loading for OPT2 is much higher around the airfoil frontal part and as a result the loading is reversed at the airfoil rear part. That is, the SS Mach number is lower than the PS Mach number. This is due to the effect of both, maximum thickness and curvature, located at the rear part, as shown in Figure 8. Therefore, it seems that the OPT2 airfoil suction surface static pressure in the rear part at mid-span is much higher than that at the hub. The largest positive static pressure gradient from hub to mid-span is at the blade rear part.

The blade suction surface static pressure contours for the baseline, OPT1 and OPT2 are shown in Figure 12. In the case of previous optimization results (OPT1 [8]) there was a strong static pressure gradient in the OGV wake region as well as in the rear part of the airfoil from tip to the hub due to the oscillatory casing profile, especially due to a second concave surface. Therefore the migration of low momentum fluid from hub region toward mid-span was significantly suppressed in the OGV wake. In the case of the present optimization (OPT2) there is no second concave surface. Instead of that, there is a higher static pressure region in the rear part of the airfoil around mid-span, due to the novel geometry of OPT2, as mentioned before. It seems that the migration of low momentum fluid along the suction surface toward mid-span is significantly suppressed for OPT2.

The numerical streaklines for the baseline, OPT1 and OPT2 are shown in Figure 13. In the case of the baseline, the migration level related to a hub corner separation extends up to about 60% span-height at TE and in the case of OPT1 (Ref. [8]) it is reached at about 40% span-height. On the other hand, in the case of OPT2, the level is less than 25% span-height. However there seems to be a higher concentrated core vortex and this seems to lead a higher loss region around hub, as already shown in Figure 10.

CONCLUSIONS

In order to find a new design concept related to an OGV blade geometry, a representation was utilized in an optimization process which is able to generate comparable larger modifications on the blade surface. The analysis of the resulting geometries presented in this paper based on 3D CFD simulations and experimental data measured for a baseline OGV blade. Three blades are compared, a baseline design and two designs resulting from numerical design optimization processes. The following conclusions can be drawn:

- The final optimized design has displayed a novel blade geometry that has a maximum blade thickness around 80% blade chord length around mid-span region, although the airfoil geometry at hub and tip region is similar to the conventional controlled diffusion airfoil.
- The main reason why the novel OGV without an oscillatory casing profile has a good performance similar to that of an earlier optimization with an oscillatory casing profile is due to the combination of conventional airfoil and the novel airfoil that generates the positive static pressure gradient on SS from hub to mid-span that is very effective for suppressing a migration of low momentum fluid on the SS for the swept OGV.

OUTLOOK

The new design concept shows, that a high reduction of the overall loss level is possible. However, currently the overall loss reduction comes at the cost of a local loss increase near the hub which might have negative impact on a LPC downstream of the OGV. Therefore, further investigations will address the effect of the blade and casing geometry on the local loss distribution in more detail.

Copyright © 2014 by ASME

REFERENCES

[1] Tweedt, D.W., Okiishi, T., and Hathaway, M.D., 1986, "Stator Endwall Leading-Edge Sweep and Hub Shroud Influence on Compressor Performance," ASME *Journal of Turbomachinery*, Vol. 108, pp. 224-232.

[2] Friedrichs, J., Baumgarten, S., Kosyna, G., and Stark, U., 2000, "Effect of Stator Design on Stator Boundary Layer Flow in a Highly Loaded Single-Stage Axial-Flow Low-Speed Compressor," ASME *Journal of Turbomachinery*, Vol. 123, pp. 483-489.

[3] Guemmer, V., Wenger, U., and Kau, H.-P., 2001, "Using Sweep and Dihedral to Control Three-Dimensional Flow in Transonic Stators of Axial Compressors," ASME *Journal of Turbomachinery*, Vol. 123, pp. 40-48.

[4] Dorfner, C., Nicke, E., and Voss C., 2007, "Axis-Asymmetric Profiled Endwall Design Using Multiobjective Optimization Linked With 3D Rans-Flow-Simulations," ASME Paper GT2007-27268.

[5] Hicks, R.M. and Henne, P.A., 1978, "Wing Design by Numerical Optimization", *AIAA Journal*, 15(7) pp.407-412.

[6] Sonoda, T., Yamaguti, Y., Arima, T., Olhofer, M., Sendhoff, B., Schreiber, H. A., 2004, "Advanced High Turning Compressor Airfoils for Low Reynolds Number Condition, Part 1: Design and Optimization", ASME *Journal of Turbomachinery*, Vol. 126, No. 3, pp.350-359.

[7] Schreiber, H.A., Steinert, W., Sonoda, T., and Arima, T., 2004, "Advanced High Turning Compressor Airfoils for Low Reynolds Number Condition, Part 2: Experimental and Numerical Analysis," ASME *Journal of Turbomachinery*, Vol. 126, No. 4, pp. 482-492.

[8] Endicott, G., Sonoda, T., Olhofer, M., and Arima, T., 2011, "Aerodynamic Improvement of A Transonic Fan Outlet Guide Vane Using 3D Design Optimization," 2011, ASME Paper GT2011-46363.

[9] Wennerstrom, A.J., 1984, "Experimental Study of a High Throughflow Transonic Axial Compressor Stage," ASME *Journal of Engineering for gas turbines and Power*, 106, pp. 552-560.

[10] Arima, T., Sonoda, T., Shirotori, M., Tamura, A., and Kikuchi, K., 1999, "A Numerical Investigation of Transonic Axial Compressor Rotor Flow Using a Low-Reynolds-Number k-ε Turbulence Model," ASME *Journal of Turbomachinery*, Vol. 121, pp.44-58.

[11] Menter, F. R., 1994, "Two-Equation Eddy-Viscosity Turbulence Models for Engineering Applications," AIAA Journal, Vol. 32, No. 8, pp. 1598-1605.

[12] Rumsey, C. L. and Spalart, P. R., 2008, "Turbulence Model Behavior in Low Reynolds Numbers Regions of Aerodynamic Flow Fields," AIAA-Paper 2008-4403.[13]

[13] Kennedy, J.; Eberhart, R. (1995). "Particle Swarm Optimization". *Proceedings of IEEE International Conference on Neural Networks*. **IV**. pp. 1942–1948. doi:10.1109/ICNN.1995.488968.

[14] Sonoda, T., Arima, T., Endicott, G., Olhofer, M., 2011, "A New Aerodynamic Design Concept for Transonic Swept Fan Outlet Guide Vanes," ISABE-2011-1224.

Copyright © 2014 by ASME

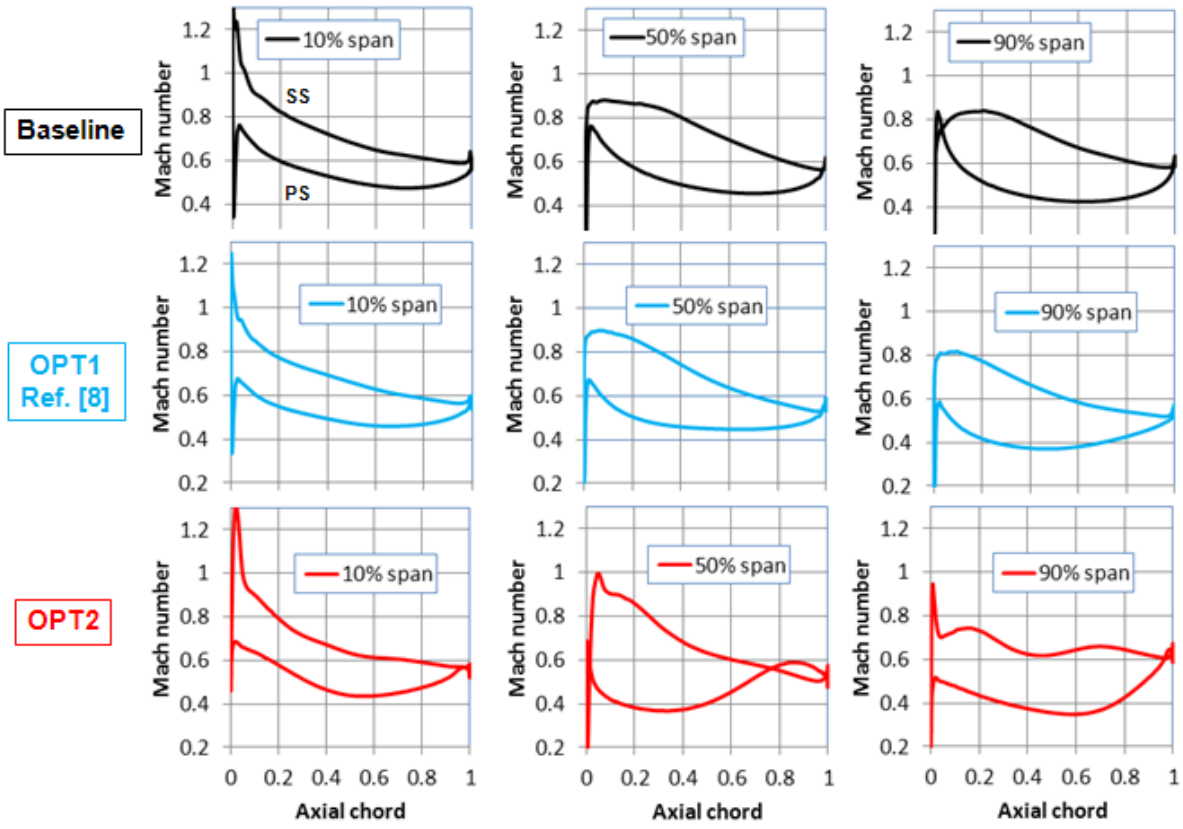

Figure 11: Numerical comparison of blade surface Mach number distributions at P2, cruise speed-line for baseline (top), OPT1 (middle, Ref. [8]) and OPT2 (bottom).

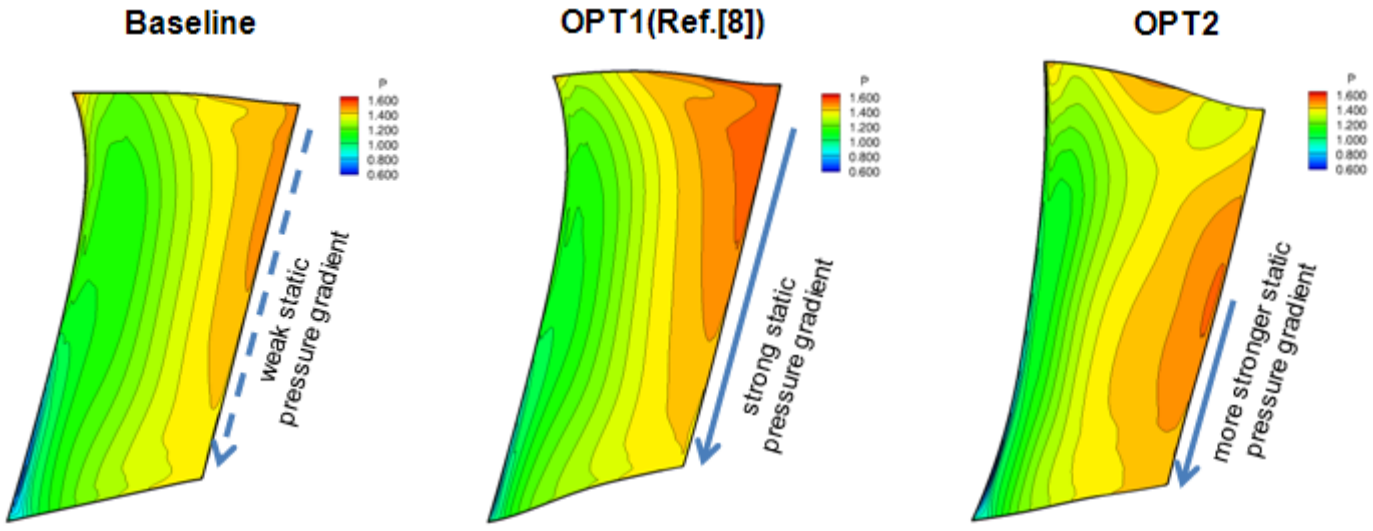

Figure 12: Numerical comparison of blade suction surface static pressure contours at P2, cruise speed-line, for baseline (left), OPT1 (middle, Ref. [8]) and OPT2 (right).

Copyright © 2014 by ASME

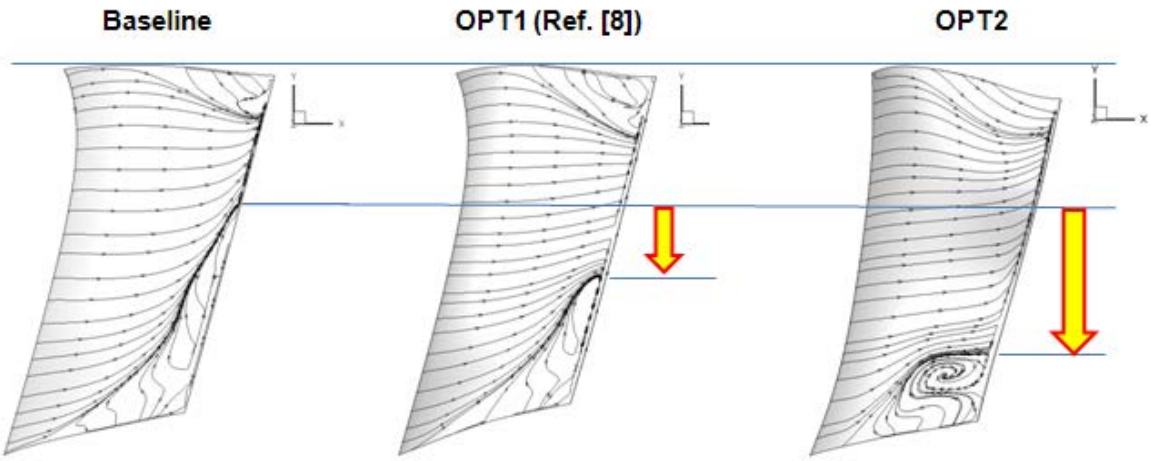

Figure 13: Numerical comparison of blade suction surface oil flow pattern at P2, cruise speed-line, for baseline (left), OPT1 (middle, Ref. [8]) and OPT2 (right).

Copyright © 2014 by ASME